AIAA Propulsion and Energy Forum
19-22 August 2019, Indianapolis, IN
AIAA Propulsion and Energy 2019 Forum

10.2514/6.2019-3873

Characterization of an integrated nozzle and supersonic axial turbine with a rotating detonation combustor

James Braun[1a], Zhe Liu[2a], David Cuadrado[3a], Valeria Andreoli[4a], Guillermo Paniagua[5 a, b], Jorge Saavedra[6a], Venkat Athmanathan[7a] and Terrence R. Meyer[8a]

[a]*Purdue University, West-Lafayette, Indiana, 47907, USA*

[b]*Petal Solutions LLC, West Lafayette, Indiana, 47907, USA*

In this work, the integration of supersonic turbomachinery with rotating detonation combustors is analyzed. First, a two-dimensional unsteady Reynolds-Averaged Navier-Stokes simulation of a rotating detonation combustor is presented and compared to experiments. The unsteady outlet of the RDC is then used as inlet condition for the 3D non-reactive URANS simulations to investigate the influence of a divergent nozzle downstream of the combustor. Influence of the nozzle on flow angle and total pressure loss during several periods of the rotating detonation wave are computed and compared with steady simulations. To further mitigate the unsteady flow behavior, supersonic stators are used and its flow field is studied. Finally, the implementation of the supersonic stator vanes in the Turbine-Integrated High-Pressure Optical RDE (THOR) test platform is described.

I. Introduction

Rotating detonation combustors (RDC) could theoretically enhance gas turbine cycle efficiency [1], however the integration of these combustors with turbomachinery plays a major role extraction of practical cycle gains. The unsteady outlet flow field from the combustor comes with aerothermal and structural challenges. Prior research demonstrated that a downstream component might affect the performance via divergent nozzles (Yi et al [2] observed a high dependence of total pressure loss on the nozzle angle) or Laval nozzles which had highest specific impulse in a study of Yetao et al. [3]. Braun et al. [4] used a reactive OpenFoam flow solver to investigate divergent nozzles with multiple expansion ratios downstream of RDCs and total pressure gain as well as Mach number and flow angle was affected by the nozzle geometry. Rankin et al. [5] studied the damping across a converging-diverging nozzle geometry subjected to periodic inlet boundary conditions derived from an RDC exhaust flow. For turbine integration purposes, one possibility is to employ a nozzle, one that increases the outlet Mach number, followed by attaching a supersonic turbine. Sousa and Paniagua [6] and Paniagua et al. [7] demonstrated that to prevent unstarting issues in supersonic flow passages downstream of combustion, the Kantrowitz limit [8] must be met and that high outlet Mach numbers are preferred. Furthermore, Sousa et al. [9] built an engine map for RDCs with supersonic axial turbines and found gains in cycle efficiency at low compression ratios. Liu et al. [10] assessed the aerodynamic performance of a supersonic turbine operating downstream of a nozzle coupled with a RDC using URANS simulations and the results

[1] PhD Candidate, School of Mechanical Engineering, Zucrow Laboratories, AIAA Student Member.

[2] PhD Candidate, School of Mechanical Engineering, Zucrow Laboratories, AIAA Student Member.

[3] Post-doctoral researcher, School of Mechanical Engineering, Zucrow Laboratories, AIAA Member.

[4] PhD Candidate, School of Mechanical Engineering, Zucrow Laboratories, AIAA Student Member.

[5] Professor, School of Mechanical Engineering, Zucrow Laboratories, AIAA Associate Fellow.

[6] Post-doctoral researcher, School of Mechanical Engineering, Zucrow Laboratories, AIAA Member.

[7] PhD Candidate, School of Aeronautics and Astronautics, Zucrow Laboratories, AIAA Student Member.

[8] Professor, School of Mechanical Engineering, Zucrow Laboratories, AIAA Associate Fellow.

demonstrated that fluctuating amplitude of supersonic flow could penalize the turbine aerodynamic performance, particularly at high frequencies.

The objective of this numerical investigation is to analyze a supersonic vane row, conceived for testing with the Turbine-Integrated High-Pressure Optical (THOR) RDE test article. Turbine inlet boundary conditions were extracted from the outlet of a 2D unfolded RDC simulation, which is validated against experimental data. Afterwards, a supersonic vane is designed and optimized by a method of characteristics solver. With 3D URANS, aerodynamic performance of the supersonic vane is evaluated in terms of total pressure loss, flow turning and damping. Finally, the proposed design is fabricated with additive manufacturing and a future experimental demonstration is outlined.

II. RDC modeling and validation

CFD++, a commercial CFD software (developed by Metacomp technologies [11]), is used to model the RDC flow characteristics. In Figure 1a, the instantaneous static temperature field of a canonical unfolded RDC is depicted. Meshing and modeling details are provided in [12]. At the inlet of the RDC, total pressure and temperature profiles were applied. Low level back pressure was imposed in the outlet and periodicity was imposed at the sides. The detonation front traveled at 1840 m/s [12] (around 6% below CJ speed). Figure 1b plots the outlet Mach number and mass-flow averaged value is transonic with peaks up to M 1.15[12].

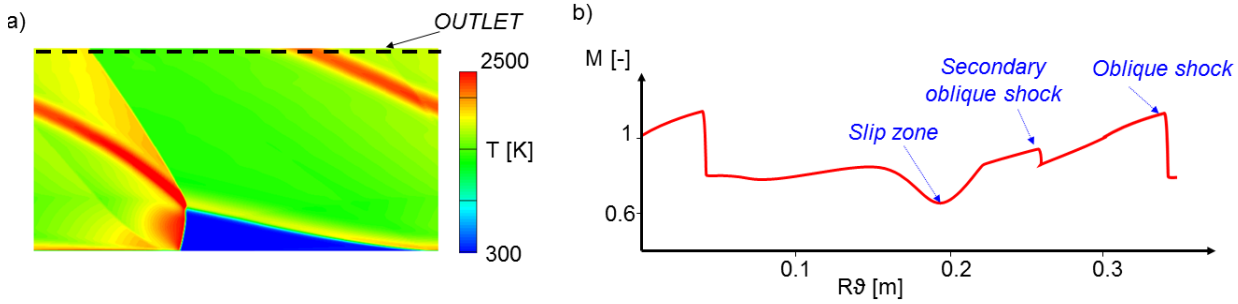

Figure 1 a) Temperature contour of a canonical unfolded RDC, b) outlet Mach number with identified shock patterns [12]

Figure 2 displays the Purdue Turbine-Integrated High-Pressure Optical RDE [13]. The RDC features a fully quartz outer-body and for these test non-preheated H_2-air were used as reactants. The design is modular to study different injection schemes and turbine configurations [13].

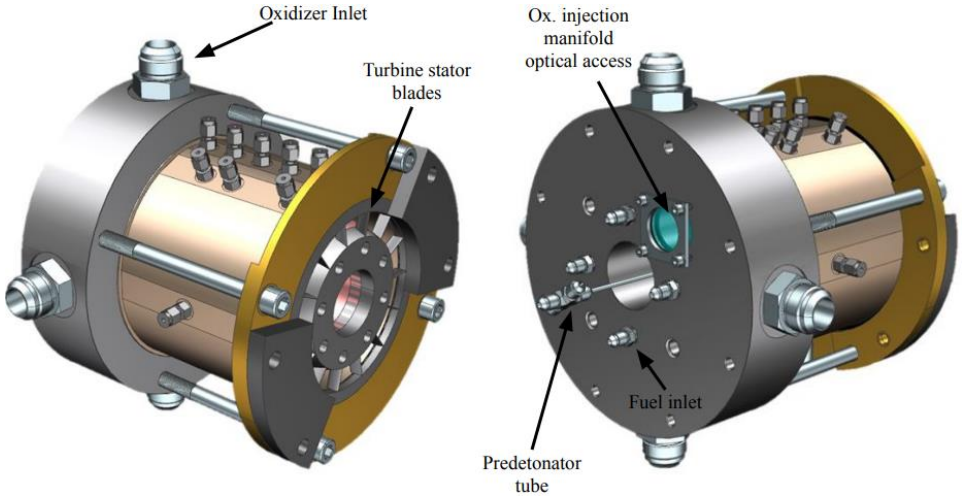

Figure 2 Turbine-Integrated High-Pressure Optical RDE (THOR) at Purdue University [13]

Figure 3a shows a visualization of a 2D unfolded RDC simulation with the same dimensions to the THOR test article flow path. At the inlet, premixed H_2-air and pure air is injected through periodically altered injection holes to model non-ideal mixing of reactants. At a certain operating condition imposed for testing and simulation, the modeled temperature field is compared with OH* filtered images (Figure 3bc), which was obtained from the optically accessible test section of THOR. The predicted refill height and oblique shock pattern match the experimental results. The detonation height in the 2D URANS is around 4 cm.

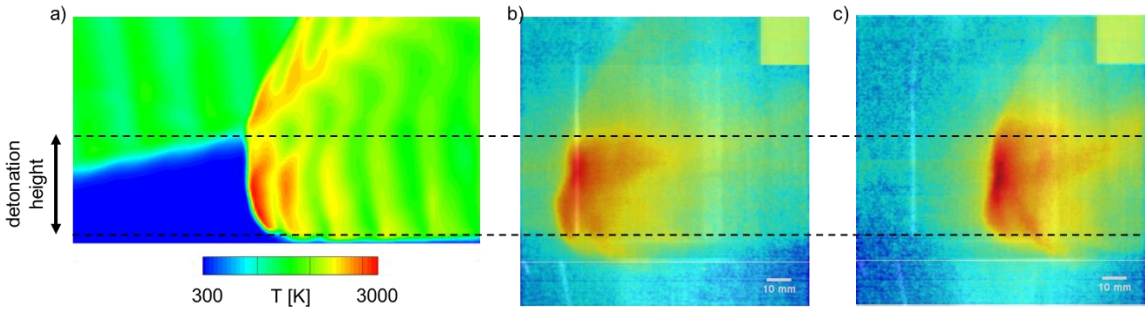

Figure 3 a) 2D RDC simulation of the THOR RDC, b) and c) OH filtered view on the refill zone, detonation front, triple point and oblique shock (exponentially scaled intensities)*

The tangential flow angle near the outlet of the RDC is visualized in Figure 4a. Flow angles reach -20 to 40 degrees at the outlet and Mach numbers fluctuate near the transonic regime. In Figure 4b, the total pressure gain (calculated as the relative difference between the inlet total pressure and the mass flow averaged total pressure at each axial location) is shown at each axial location. The pressure gain peaks at the triple point with values around 2 and decays due to the pressure loss associated to the rotating oblique shock. The min-to-max flow angle is plotted in Figure 4c. The flow angle variation drops from 150 degrees to around 70 at the outlet. Hence, a nozzle and/or supersonic vanes need to be used to further mitigate the flow angle fluctuations to the rotor inlet.

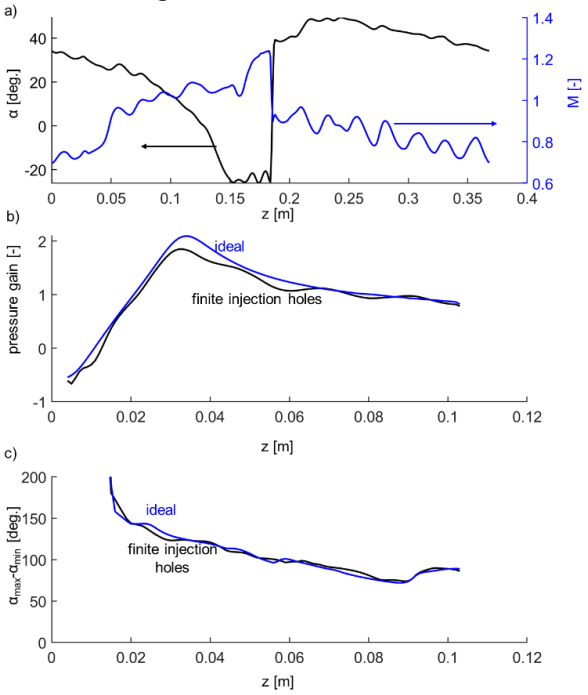

Figure 4 RDC: a) Flow angle and Mach number at the outlet of the RDC, b) total pressure gain in function of the axial distance of the RDC and c) min-to-max flow angle in function of the axial position

III. Uncoupling of the RDC combustor and downstream component

To analyze the downstream component of the RDC, the outlet conditions of the RDC were extracted and used as transient inlet condition to a smoothly diverging nozzle, identical to the one described by Braun et al. [13]. To demonstrate the validity of this approach, Figure 5 plots the mass-flow averaged total pressure as a function of the axial distance for two simulations. The first simulation (red curve) represents the two-dimensional unsteady reactive simulation of the RDC. The outlet conditions, which were extracted at 0.15m, were then used as inlet condition to a three dimensional simulation (blue curve) and a similar total pressure decay is obtained.

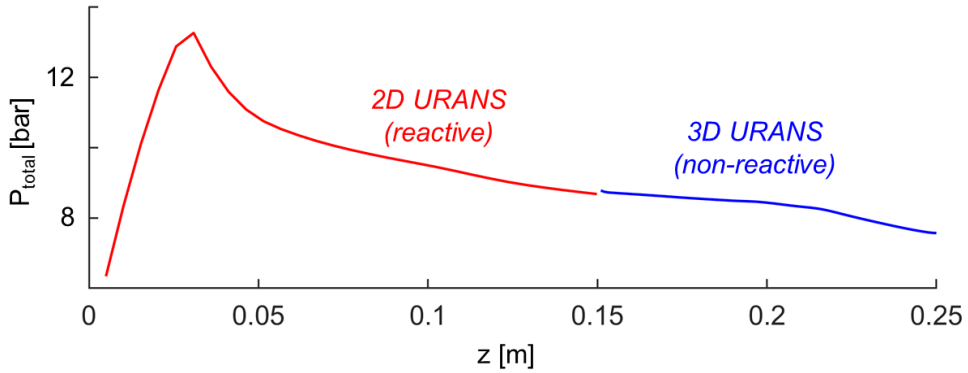

Figure 5: Losses in the RDC: mass-flow averaged total pressure in function of the axial distance

A mass-flow averaged steady simulation of the smooth diverging nozzle is visualized in Figure 6a with the unsteady rotating shock being shown in Figure 6b where the flow field is color coded by Mach number. We can see that high local temporal discrepancies in pressure and Mach number are observed due to the presence of the sweeping shock.

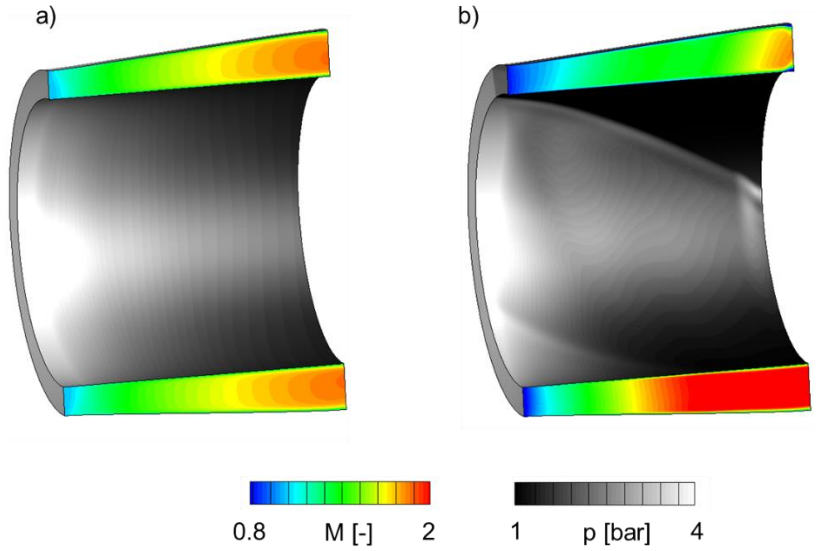

Figure 6: a) nozzle exposed to steady supersonic flow and b) nozzle exposed to the rotating detonation shock

To take a closer look at the total pressure loss due to the oblique shock, Figure 7 plots the mass-flow averaged total pressure loss at each axial location. After 8 cm, total pressure loss is around 15%, while for a steady case the total pressure near the outlet is only 6%. The discrepancy is due to the rotating shock, which induces additional losses driven by the unsteady pressure wave interactions. For this reason, short nozzles are preferred. The min-to-max flow angle is plotted and shows a reduction from 55 degrees to 37 degrees. However, the flow angle still contains positive and negative contributions with a mass-flow averaged value below few degrees.

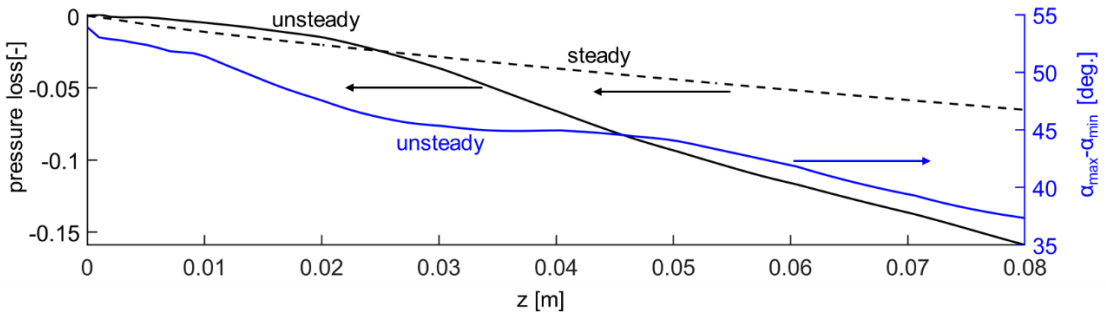

Figure 7: total pressure loss and flow angle distribution for the steady and unsteady case

Due to the fact that negative flow angles are still present and cannot be eliminated in short nozzles, a vane row is required to efficiently guide the flow and set a rather uniform flow angle.

IV. Supersonic Turbine: characterization of the losses

A supersonic stator was designed and optimized by a method of characteristics design tool [6]. The stator profile was shortened by half and re-enforced at the leading edge considering the high transient heat- and structural loads of the RDC to which the stator will be exposed. Flow turning was constrained by 12 degrees, and pressure side and suction side were parametrized by a 3rd-order Bezier polynomial to ensure smooth curves. Figure 8a depicts the channel variation from stator inlet to outlet, where the channel height was increased by 22% to enhance the self-starting capability and power extraction. A smooth diverging curve to enhance damping and flow momentum [12] was used along the axial distance downstream of the RDC. The numerical grid for a single passage is displayed in Figure 8b, with a close-up view of the stator trailing edge grid topology shown in Figure 8c. The turbulence model was provided with the k-w SST, and the non-dimensional first layer thickness (y+) was lower than 1 to ensure the viscous sublayer was accurately predicted. For steady cases, constant static pressure, static temperature, and velocity components were prescribed at stator inlet.

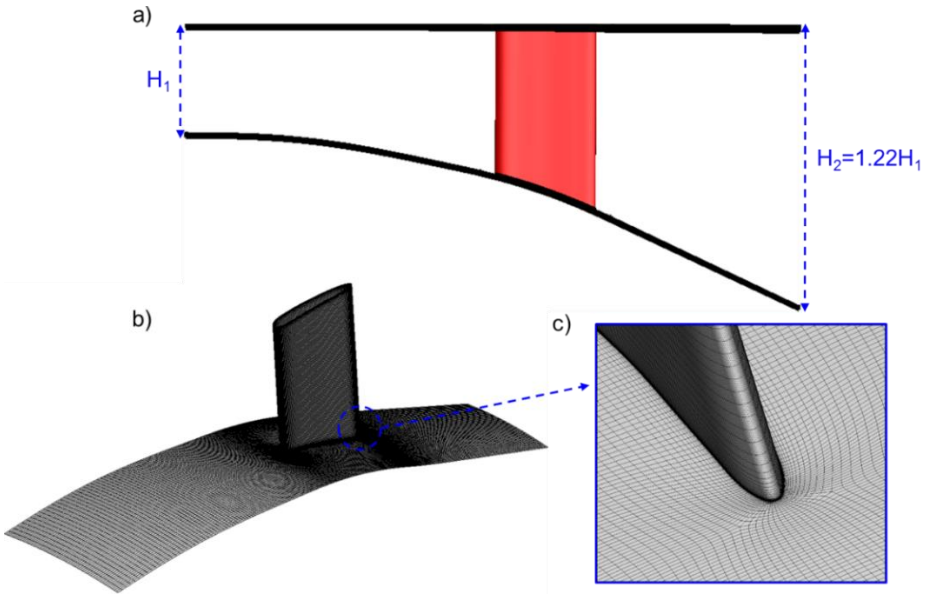

Figure 8: Supersonic stator design, a) cross-sectional view of the stator, b) mesh of one stator and c) zoom on the trailing edge

A mesh sensitivity analysis was performed with four mesh sizes ranging from 0.95 million to 2.95 million mesh cells. Figure 9 represents total pressure loss evaluated at different mesh sizes, with a discrepancy of 0.2 percentage-point going from medium to fine mesh. Hence, fine mesh with around 2.95 million mesh cells was selected for the investigation.

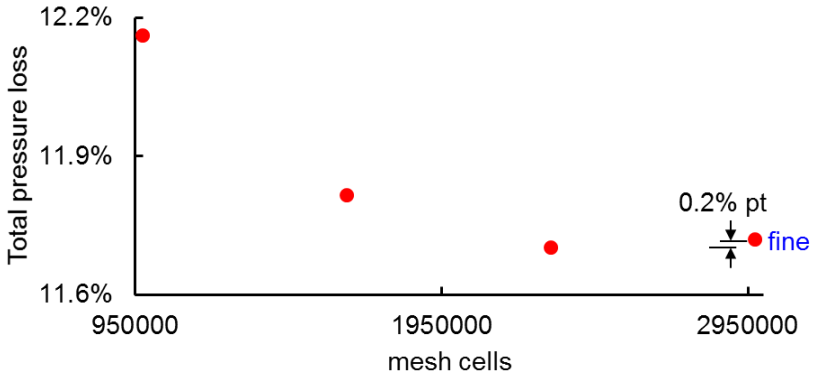

Figure 9: Total pressure loss in function of mesh cell count

The performance comparison between the long-thin and short-re-enforced design with the same vane count is illustrated in Figure 10. The total pressure loss increases by 2.4 percentage-points from the thin (Figure 10a) to the re-enforced (Figure 10b) stator profile due to higher shock loss introduced by the larger leading edge thickness.

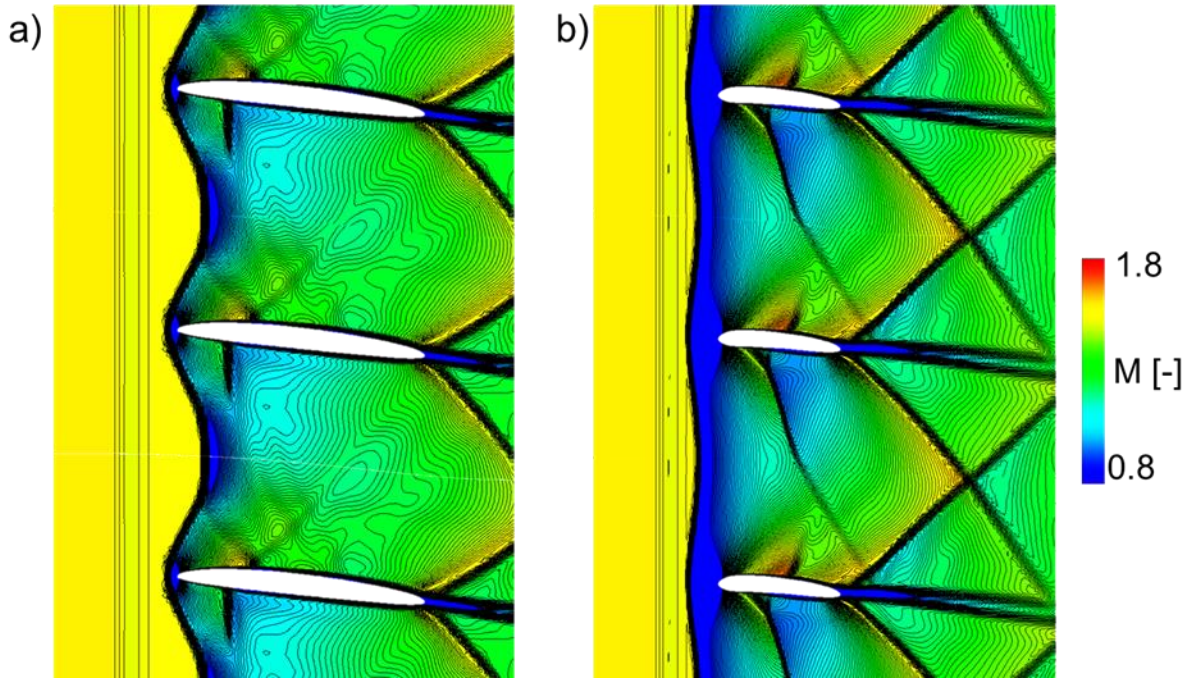

Figure 10: Mid-span steady state Mach contour for a) thin supersonic stator, b) re-enforced shorter version to be tested in the THOR facility

The designed supersonic stator is required to guarantee self-starting capability in the transonic regime downstream of RDCs. To characterize the unsteady operation of this design exposed to RDC outflow, the instantaneous outlet profile of a 2D unfolded RDC was imposed at stator inlet, similar to the strategy used in the nozzle [13]. Figure 11a illustrates the time-resolved mid-span flow field of the supersonic stator exposed to a periodic oblique shock. The inlet oblique shock tangentially sweeps from the stator suction side to the pressure side, creating shock reflections and interactions within the stator passage. Flow turning is opposite to the inlet oblique shock angle, therefore high pressure flow behind the inlet shock is well guided by the stator. A detail on the shock structure within the stator passage is illustrated in Fig. 11b. At point ‘A’, two leading edge reflected shocks interact and lead to two oblique shocks. One oblique shock impinges on the trailing edge shock from the pressure side at point ‘B’. The other shock strikes on the suction side trailing edge shock at point ‘C’. Further downstream, the trailing edge shocks merge and exit toward the outlet.

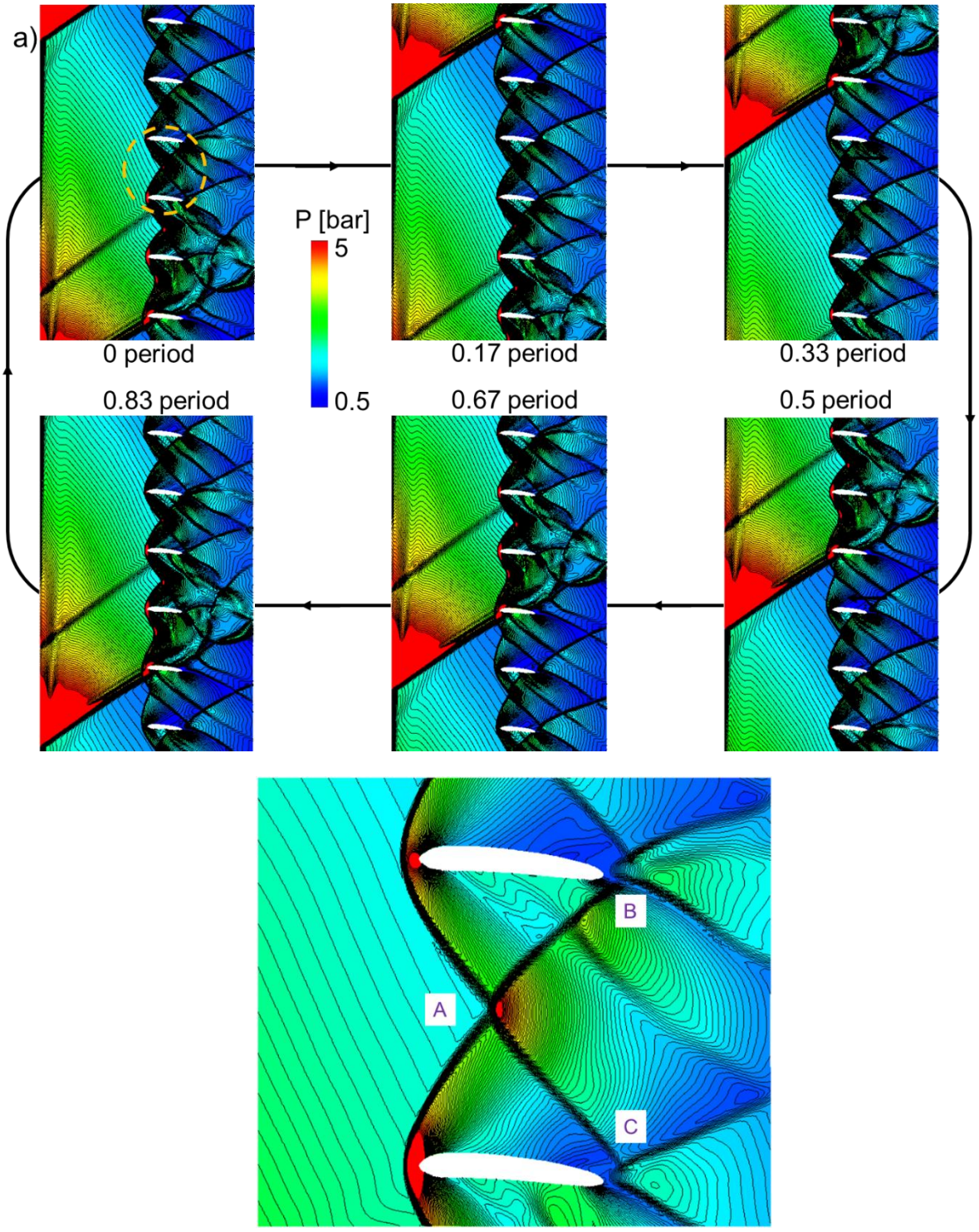

Figure. 11 a) Instantaneous stator mid-span pressure contour during one oblique shock period. b) Zoomed view of instantaneous shock structure within the stator passage

A vital feature for stator passages is the attenuation of large unsteady oscillations in order to guarantee the rotor self-starting. Taking advantage of the stator flow angle variation mitigation, the rotor suffers lower losses and delivers high power output. Figure 12 plots the instantaneous variations of mass-flow-averaged flow angle (Figure 12a), static pressure (Figure 12b), Mach number (Figure 12c), and static temperature (Figure 12d) along the tangential direction of the stator inlet and outlet for two different vane counts: 16 vanes and 24 vanes. Instantaneous damping is defined

in Eq. 1 to quantify the attenuation of fluctuations across the stator. As the vane count increases from 16 to 24, damping of angular fluctuations increases by 45 percentage-points while the Mach number fluctuations rise by a factor of 4. Damping of static temperature peak to peak variation is augmented by 20%. In addition, time-averaged of mass-flow-averaged flow turning is enhanced by 61.5% to 8.8 degrees. However, time-averaged of mass-flow-averaged total pressure loss increases by 3 percentage-points due to the increased level of shock reflection within the passages. In general, increasing the vane count benefits the damping, providing higher flow turning, and delivering less distorted outlet profile to the rotor, but introducing higher aerodynamic losses. Additionally, very high vane counts might lead to unstarting of the flow where the inlet Mach number is close to the transonic regime.

$$Damping = \frac{std_1 - std_2}{std_1} \qquad Eq.1$$

Where 'std' represents the standard deviation.

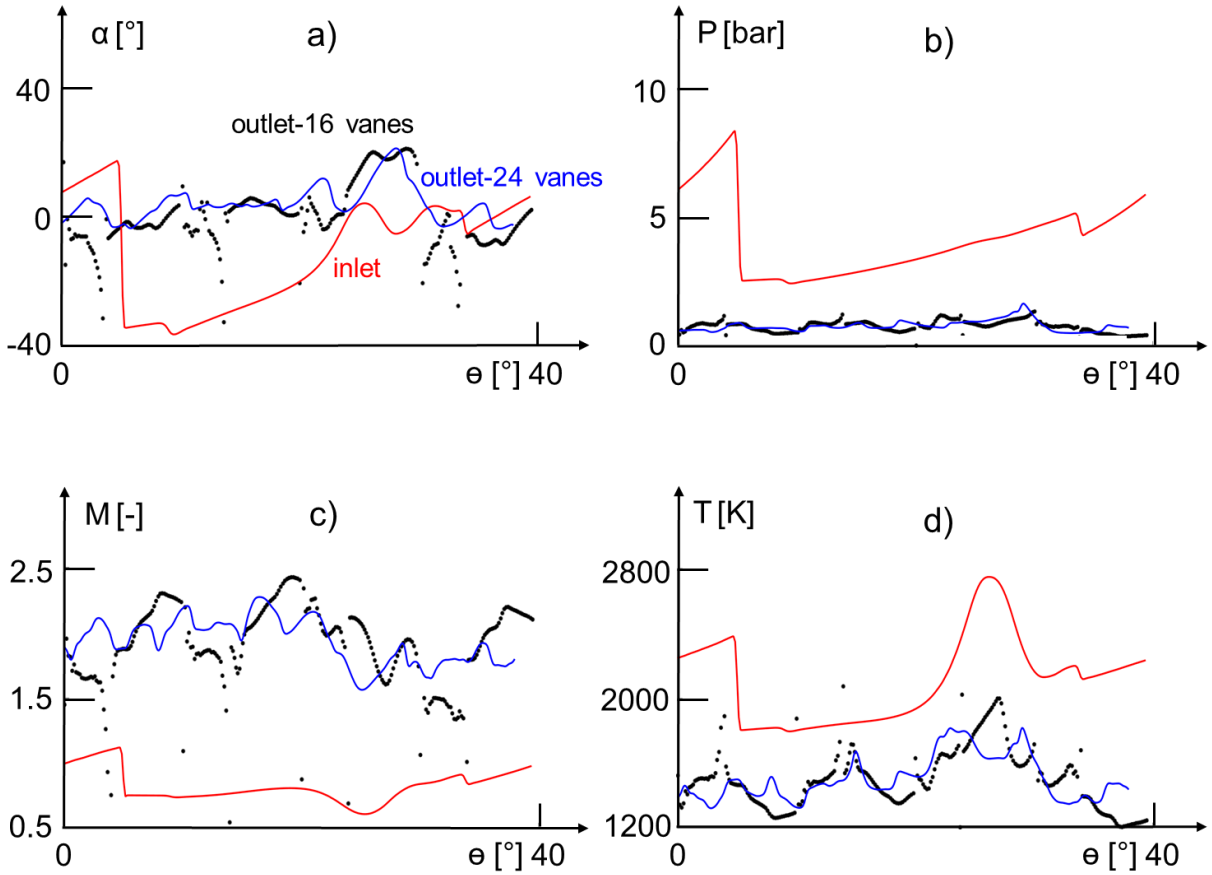

Figure 12: Inlet conditions to the stator vs outlet conditions to the stator for a) the flow turning, b) static pressure, c) Mach number and d) static temperature

Figure 13 displays the total pressure loss (Figure 13a) and flow turning (Figure 13b) as a function of the pitch-to-chord ratio for several steady inlet Mach numbers as well as for the unsteady case in which the stator is exposed to the RDC outlet conditions. The large inlet fluctuations cause higher total pressure loss. Due to the angular fluctuations at the stator inlet, time-averaged of mass-flow averaged flow turning is increased to 5.5 degrees for 16 vanes and 8.8 degrees for 24 vanes. At the same inlet Mach number, a decreased pitch-to-chord ratio introduces more shock reflection, which leads to higher total pressure losses. However, lower pitch-to-chord ratio provides better flow guidance and results in higher flow turning. At the same pitch-to-chord ratio, a higher inlet Mach number is associated to higher shock intensity causing higher total pressure losses.

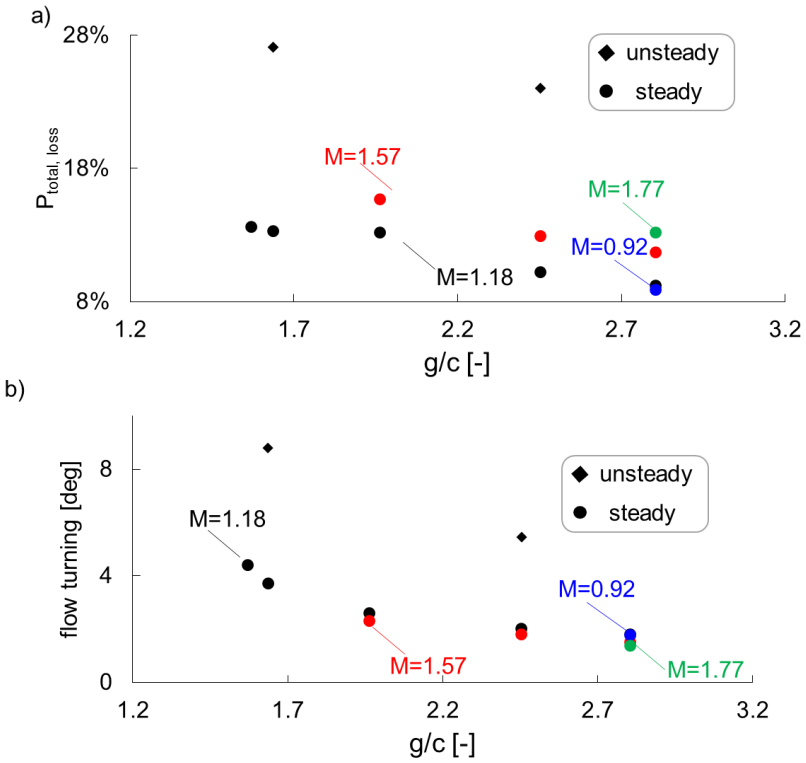

Figure 13: Influence of pitch-to-chord on a) total pressure loss, and b) flow turning

V. Manufacturing of the turbine

The manufactured blade is displayed in Figure 14. Manufacturing was performed by Innovative 3D Manufacturing LLC. This row of stator blades will be tested in the future and flow angle as well as total pressure loss will be measured to validate the unsteady CFD and propose corrections models.

Figure 14 Additive manufactured vane row

VI. Conclusions

In this work, the outlet conditions of a Rotating Detonation Combustor were conditioned to enable power extraction from a supersonic turbine. To increase the Mach number and reduce flow angle variations at the outlet of the combustor, a smooth divergent nozzle was deployed upstream of the turbine stages. Eight centimeters downstream of the RDC, pressure loss was estimated to be 16% for an unsteady simulation while only 8% loss was observed in the case of a steady simulation. The presence of the unsteady pressure wave interactions exacerbated the pressure losses. It was observed that flow angle oscillations could not be reduced further through the nozzle. In order to mitigate further flow variations, a supersonic stator vane row was introduced downstream of the expansion nozzle. This supersonic vane row was analyzed and conceived for testing in the Turbine-Integrated High-Pressure Optical (THOR) facility. Turbine inlet boundary conditions were extracted from the outlet of a 2D unfolded RDC simulation and the detonation height and oblique shock angle matched with OH* imaging from the experiments. With 3D URANS, the aerodynamic performance of the supersonic vane is evaluated in terms of total pressure loss, flow turning and damping. Higher flow turning at the outlet of the vane were successfully achieved with 24 vanes and the flow through the vane passage was still started. The unsteady simulations of the passage were also compared to steady simulations and a penalty of around 10% in total pressure loss was found.

VII. Nomenclature

α	Flow angle [deg]
c	Axial chord length [m]
g	Pitch [m]
H	Channel height [m]
M	Absolute Mach number [-]
P	Static pressure [bar]
P_{total}	Total pressure [bar]
std	Standard deviation [-]
T	Static temperature [K]
θ	Azimuthal angle [deg]
z	Axial length [m]

Abbreviation

CFD	Computational fluid dynamics
RDC	Rotating detonation combustor
URANS	Unsteady Reynolds-Averaged Navier-Stokes
THOR	Turbine-Integrated High-Pressure Optical RDE

VIII. Nomenclature

The authors wish to acknowledge Jordan Fisher and Zachary Ayers for their help in the THOR test campaign.

IX. References

[1] Heiser, W. H., and Pratt, D. T., 2002, "Thermodynamic Cycle Analysis of Pulse Detonation Engines. Journal of Propulsion and Power," Vol. 18, No. 1, pp 68-76. doi: https://doi.org/10.2514/2.5899

[2] Yi, T.-H., Lou, J., Turangan, C., Khoo, B. C., and Wolanski, P., 2010, "Effect of Nozzle Shapes on the Performance of Continuously Rotating Detonation Engine," Proceedings of 48th AIAA Aerospace Sciences Meeting Including the New Horizons Forum and Aerospace Expositions, Jan 4-7, Orlando, FL. doi: https://doi.org/10.2514/6.2010-152

[3] Shao, Y., Liu, M., and Wang, J.-P., 2010, "Continuous Detonation Engine and Effects of Different Types of Nozzle on Its Propulsion Performance," Chinese Journal of Aeronautics, Vol. 23, No. 6, pp. 647–652. doi: https://doi.org/10.1016/S1000-9361(09)60266-1

[4] Braun, J., Saracoglu, B.H., and Paniagua, G., 2016, "Unsteady Performance of Rotating Detonation Engines with Different Exhaust Nozzles," Journal of Propulsion and Power, Vol. 33, No. 1, pp. 1-10. doi: https://doi.org/10.2514/1.B36164

[5] Rankin, B.A., Hoke, J., and Schauer, J., 2014, "Periodic Exhaust Flow through a Converging-Diverging Nozzle Downstream of a Rotating Detonation Engine," Proceedings of 52nd Aerospace Sciences Meeting, Jan 13-17, Nantional Harbor, ML. doi: http://doi.org/10.2514/6.2014-1015

[6] Sousa, J., and Paniagua, G., 2015, "Entropy Minimization Design Approach of Supersonic Internal Passages," Entropy, Vol. 17, No. 8, pp. 5593-5610. doi: https://doi.org/10.3390/e17085593

[7] Paniagua, G., Iorio, M.C., Vinha, N., and Sousa, J., 2014, "Design and Analysis of Pioneering High Supersonic Axial Turbines," International Journal of Mechanical Sciences, Vol. 89, pp. 65–77. doi: https://doi.org/10.1016/j.ijmecsci.2014.08.014

[8] Kantrowitz, A., and Donaldson, C., 1945, "Preliminary Investigation of Supersonic Diffusers," National Advisory Committee for Aeronautics, NACA-WR-L-713.

[9] Sousa, J., Paniagua, G., and Morata, E.C., 2017, "Thermodynamic analysis of a gas turbine engine with a rotating detonation combustor," Applied Energy, Vol. 195, pp. 247–256, doi: https://doi.org/10.1016/j.apenergy.2017.03.045

[10] Liu, Z., Braun, J., and Paniagua, G., 2019, "Characterization of A Supersonic Turbine Downstream of A Rotating Detonation Combustor," Journal of Engineering for Gas Turbines and Power, Vol. 141, No. 3, doi: https://doi.org/10.1115/1.4040815

[11] Chakravarthy, S., Peroomian, O., Goldberg, U., and Palaniswamy, S., 1998, "The CFD++ Computational Fluid Dynamics Software Suite," SAE Technical Paper 985564, DOI: https://doi.org/10.4271/985564

[12] Braun, J., Saavedra, J., and Paniagua, G., 2017, "Evaluation of the unsteadiness across nozzles downstream of rotating detonation combustors," Proceedings of 55th AIAA Aerospace Sciences Meeting, Jan 9-13, Grapevine, TX. doi: https://doi.org/10.2514/6.2017-1063

[13] Athmanathan, V., Fisher, J., Ayers, Z. M., Cuadrado, D.G., Andreoli, V., Braun, J., Meyer, T., Paniagua, G., Fugger, C.A., and Roy, S., 2019, "Development of a turbine-integrated high-pressure optical RDE (THOR) for time-resolved fluid dynamic measurements using high-speed optical diagnostics," Proceedings of 55th AIAA/SAE/ASEE Joint Propulsion Conference, Aug 19-22, Indianapolis, IN